



**HAL**  
open science

## Acquired resistance to a GPRC5D-directed T-cell engager in multiple myeloma is mediated by genetic or epigenetic target inactivation

Jennifer Derrien, Sarah Gastineau, Antoine Frigout, Nils Giordano, Mia Cherkaoui, Victor Gaborit, Rémi Boinon, Elise Douillard, Magali Devic, Florence Magrangeas, et al.

### ► To cite this version:

Jennifer Derrien, Sarah Gastineau, Antoine Frigout, Nils Giordano, Mia Cherkaoui, et al.. Acquired resistance to a GPRC5D-directed T-cell engager in multiple myeloma is mediated by genetic or epigenetic target inactivation. *Nature Cancer*, In press, 10.1038/s43018-023-00625-9 . hal-04265728

**HAL Id: hal-04265728**

**<https://hal.science/hal-04265728>**

Submitted on 6 Nov 2023

**HAL** is a multi-disciplinary open access archive for the deposit and dissemination of scientific research documents, whether they are published or not. The documents may come from teaching and research institutions in France or abroad, or from public or private research centers.

L'archive ouverte pluridisciplinaire **HAL**, est destinée au dépôt et à la diffusion de documents scientifiques de niveau recherche, publiés ou non, émanant des établissements d'enseignement et de recherche français ou étrangers, des laboratoires publics ou privés.

# Acquired resistance to a GPRC5D-directed T cell engager in multiple myeloma is mediated by genetic or epigenetic target inactivation

Jennifer Derrien<sup>1\*</sup>, Sarah Gastineau<sup>1\*</sup>, Antoine Frigout<sup>1</sup>, Nils Giordano<sup>1</sup>, Mia Cherkaoui<sup>1</sup>, Victor Gaborit<sup>1,2</sup>, Rémi Boinon<sup>1</sup>, Elise Douillard<sup>1,2</sup>, Magali Devic<sup>1,2</sup>, Florence Magrangeas<sup>1,2</sup>, Philippe Moreau<sup>1,3</sup>, Stéphane Minvielle<sup>1,2</sup>, Cyrille Touzeau<sup>1,3</sup> & Eric Letouzé<sup>1,2</sup>

1 Nantes Université, INSERM, CNRS, Université d'Angers, CRCI2NA, Nantes, France

2 University Hospital Hôtel-Dieu, Nantes, France

3 Hematology Department, University Hospital Hôtel-Dieu, Nantes, France.

\* These authors contributed equally to this work

Corresponding author: Eric Letouzé, eric.letouze@inserm.fr

## Abstract

**Bispecific antibodies targeting GPRC5D demonstrated promising efficacy in multiple myeloma, but acquired resistance usually occurs within a few months. Using a single-nucleus multi-omic strategy in 3 patients from the MYRACLE cohort (ClinicalTrials.gov identifier NCT03807128), we identified two resistance mechanisms, by bi-allelic genetic inactivation of *GPRC5D*, or by long-range epigenetic silencing of its promoter and enhancer regions. Molecular profiling of target genes may help guiding the choice of immunotherapy and early detection of resistance in multiple myeloma.**

Bispecific antibodies (BsAb) are monoclonal antibodies that redirect T cells by targeting both the T cell co-receptor CD3 and markers expressed on the surface of tumor cells<sup>1</sup>. BsAb targeting B-cell maturation antigen (BCMA, teclistamab) or G protein-coupled receptor, family C, group 5, member D (GPRC5D, talquetamab) demonstrated favorable safety profiles and promising efficacy in relapsed or refractory multiple myeloma (RRMM) in recent phase 1-2 studies<sup>2,3</sup>. However, ~30% of patients did not respond, and half of the responders experienced disease progression within 12 months. Thus, it is crucial to understand the mechanisms of innate and acquired resistance to BsAb.

Here, we explore the mechanisms of acquired talquetamab resistance in three RRMM patients from the MYRACLE cohort (ClinicalTrials.gov identifier NCT03807128)<sup>4</sup>. The 3 patients had previously received multiple therapy lines including immunomodulatory agents, proteasome inhibitors, dexamethasone and anti-CD38 antibodies (**Supplementary Table 1**). We conducted a multi-omic characterization of myeloma cells, before talquetamab treatment (t1) and after relapse (t2), by whole genome sequencing (WGS) and single-nucleus Multiome allowing simultaneous profiling of gene expression (RNA-seq) and open chromatin (ATAC-seq) from the same cells.

MM-01-0288 was a female patient diagnosed with immunoglobulin G (IgG) myeloma at 64 yo. After 4 previous therapy lines in 5.3 years, she was enrolled in the phase 1 MonumentAL-2 trial (ClinicalTrials.gov identifier NCT05050097) and received talquetamab (weekly subcutaneous injection of 400 mg/kg until progression) in combination with carfilzomib. She achieved very good partial response but the disease progressed after 6 months. WGS at t1 revealed clonal t(4;14), 1q gain, 13q loss and a focal heterozygous deletion at 12p

encompassing *GPRC5D* locus, so that a single allele remained in tumor cells (**Fig. 1a** and **Extended Data Fig. 1a,b**). This tumor was heavily mutated (31,410 somatic mutations), with a high contribution of clock-like and APOBEC mutational processes (**Extended Data Fig. 2a-c**). Driver mutations included *KRAS* G12R, *RB1* R787\* and *CDKN1B* N61I (**Supplementary Table 2**). These mutations were present in a subclone, representing 91% of tumor cells at t1 but only 24% at t2 (subclone A). By contrast, subclone B, comprising *RB1* L572fs and *HUWE1* P3841L mutations, was minor at t1 (8% of tumor cells) but became dominant at t2 (70%). Finally, the t2 sample had acquired 7 subclonal *GPRC5D* alterations: 3 frameshift indels (E27fs, S125fs, F158fs), 2 nonsense mutations (W217\*, W237\*), an in-frame deletion of 4 amino acids within transmembrane helix 3 (G97-F100), and a 10 kb deletion encompassing the transcription start site (**Extended Data Fig. 1b**). Since a single copy of *GPRC5D* remains in tumor cells, each alteration was present in a distinct subclone, representing between 6.2% and 31.6% of tumor cells (**Fig. 1b**). These alterations are predicted to prevent the translation of a functional GPRC5D protein able to be embedded in the cell membrane. Although mRNA expression was maintained (**Extended Data Fig. 3a-c**), flow cytometry confirmed the absence of GPRC5D protein at the surface of t2 cells (**Extended Data Fig. 4** and **Extended Data Fig. 5a-c**).

We next mapped clonal and subclonal genetic mutations (**Extended Data Fig. 6a**) in single-nucleus data to refine the clonal architecture of MM-01-0288, and its evolution during treatment. Single-nucleus RNA-seq revealed heterogeneous subclones, in particular at t2 (**Extended Data Fig. 6b**). Trunk somatic mutations were detected in all cells. By contrast, subclonal mutations allowed to follow subclones before and after treatment: subclone A mutations were detected in the dominant t1 subclone and 2 minor subclones at t2, whereas subclone B mutations were detected in the minor t1 subclone and the 3 largest t2 subclones (**Extended Data Fig. 6c**). Virtual copy-number analysis revealed clonal and subclonal chromosome aberrations (-1p, -10p, -14q, -14qtel, +17q and -21), consistent with WGS data (**Extended Data Fig. 7a-c**), that defined 5 subclones (cn1 to cn5, **Fig. 1c** and **Extended Data Fig. 8a-d**). Copy-number subclones largely overlapped transcriptomic clusters and refined the clonal relationships inferred from somatic mutations (**Fig. 1d**). Differentially expressed genes and pathways were consistent with subclonal genetic events, e.g. with an up-regulation of 17q genes and the Ras signaling pathway in the cn1 subclone that displays +17q and *KRAS* mutation (**Supplementary Tables 3** and **4**). Finally, we mapped *GPRC5D* alterations in single-nucleus data (**Fig. 1e** and **Extended Data Fig. 9**). Each alteration was detected in a single copy-number subclone: S125fs in cn3, F158fs in cn4 and all other alterations in the subclone cn5. Talquetamab resistance in cn2, the only subclone without a second hit in *GPRC5D*, could involve a combination of low frequency genomic alterations undetectable at this coverage, and/or post-transcriptional mechanisms precluding the protein to be translated or presented on the cell surface. Overall, integrating WGS and single-nucleus data allowed us to reconstruct the clonal evolution of this tumor, with the emergence of 7 resistant subclones harboring distinct *GPRC5D* alterations (**Fig. 1f**). Thus, in this patient with a 12p deletion at baseline, talquetamab resistance involved the independent acquisition of second hits in *GPRC5D* by several subclones, leading to the bi-allelic inactivation of the target.

MM-01-0221 (female, diagnosed with light chain myeloma at 67 yo) and MM-01-0302 (male, diagnosed with light chain myeloma at 52 yo) were enrolled in the phase 1 MonumentAL-1 trial (ClinicalTrials.gov identifier NCT03399799) and received talquetamab (weekly subcutaneous injection of 400 mg/kg until progression) after 5 (resp. 7) previous lines. They

achieved partial response for 5 (resp. 4) months before relapse (**Fig. 2a**). WGS revealed clonal t(11;14) in both cases, a bi-allelic *TP53* inactivation in MM-01-0221, and driver *KRAS*, *DUSP2* and *SETD2* mutations in MM-01-0302, but no alteration of *GPRC5D* locus in the relapse in either case (**Extended Data Fig. 10a**). By contrast, bulk RNA-seq revealed a drastic silencing of *GPRC5D* expression in both relapses (**Fig. 2b,c**), although the gene was highly expressed at t1 in MM-01-0221 (210 transcripts per million vs. 1.3 at relapse, fold-change=0.0062, no t1 data for MM-01-0302). Single-nucleus RNA-seq confirmed the lack of *GPRC5D* transcript in >99.8% of both MM-01-0221 and MM-01-0302 cells at t2 (**Extended Data Fig. 10b**). In absence of genetic insult, we examined the chromatin landscape at *GPRC5D* locus. Normal bone marrow and 7 other MM samples used as controls displayed a major ATAC-seq peak (open chromatin) at *GPRC5D* promoter, and 5 minor peaks along the gene, all of which were closed in MM-01-0221 and MM-01-0302 t2 samples (**Fig. 2b** and **Extended Data Fig. 10c**). This significant loss of chromatin accessibility was not restricted to *GPRC5D* but involved 51 chromatin accessibility peaks in an extended 1.15 Mb region around the gene (**Fig. 2d** and **Supplementary Table 5**). Thirty-five of these peaks were annotated as enhancers in ENCODE cis-regulatory element database<sup>5</sup>, 18 were found to interact with *GPRC5D* promoter in B cell promoter capture Hi-C data<sup>6</sup> and 6 were annotated as *GPRC5D* enhancers in GeneHancer database<sup>7</sup> (**Fig. 2d**). Finally, peak-to-gene expression linkage analysis in the 65,700 cells (2 normal plasma cell and 9 MM samples) revealed 12 peaks linked with *GPRC5D* expression, 9 of which were closed in our 2 *GPRC5D*-silenced relapses, including 7 ENCODE enhancers. Thus, acquired talquetamab resistance in this patient involved long-range epigenetic silencing of *GPRC5D* locus, with coordinated chromatin silencing of its promoter and enhancer regions.

In conclusion, we report two mechanisms of acquired talquetamab resistance resulting from the genetic or epigenetic inactivation of the target. The simultaneous growth of 7 resistant subclones in MM-01-0288 illustrates the ease with which tumor cells with a pre-existing chromosome 12p deletion can acquire resistance with a second hit in *GPRC5D*. These findings mirror previous results indicating that chromosome 16p deletion may increase the risk of BCMA CAR-T resistance<sup>8,9</sup>. In 752 newly diagnosed MM analyzed by WGS<sup>10</sup>, chromosome arm 12p was lost in 10%, and arm 16p in 18% of cases. Future studies of larger cohorts will be needed to establish whether these deletions predict response to bispecific antibodies and must be screened to select the best treatment option. *GPRC5D* is surrounded by inactive chromatin domains (H3K27Me3, **Fig. 2d**). This may favor its silencing by redistribution of inactive chromatin marks, as previously reported in other cancers<sup>11</sup>. Future studies will need to address whether *GPRC5D* expression before treatment influences talquetamab response. We anticipate that a thorough genetic, epigenetic and transcriptomic profiling of the targets will be important to select the most adapted bispecific antibody for each patient, and to detect early the emergence of resistant subclones.

## Methods

This research project complies with all relevant ethical regulations. The study protocol was approved by the ethics committee 'Comité de Protection des Personnes - Tours - Région Centre - Ouest 1' on July 31 2018 (2018 T3– 11 (RC18\_0197) (2018-A01578–47) (18.07.03.46219).

## Description of the cohort

We analyzed multiple myeloma samples from 3 patients included in the observational prospective cohort MYRACLE (ClinicalTrials.gov identifier NCT03807128)<sup>4</sup> between may 2021 and august 2022, before talquetamab treatment (t1) and after relapse (t2). The 3 patients received talquetamab weekly at the recommended dose of 400 mg/kg until disease progression, in the context of phase 1 clinical trials MonumentAL-1 (ClinicalTrials.gov identifier NCT03399799) and MonumentAL-2 (ClinicalTrials.gov identifier NCT05050097). Tumor response was evaluated according to international consensus criteria<sup>12</sup>. The duration of response was defined as the time between initial response and the first documented evidence of progressive disease per International Myeloma Working Group criteria. Five other myeloma patients from MYRACLE cohort were included for comparison (**Supplementary Table 6**). Bone marrow samples were collected by the Hematology department of CHU Nantes during diagnosis or follow-up visits. They were analyzed by single-nucleus Multiome to examine the expression and chromatin accessibility of *GPRC5D* in MM not treated with talquetamab, and by whole genome sequencing to determine their driver alterations. All patients provided signed informed consent to join the study (without compensation). Sex was not considered in the study design. The sex of participants was determined based on self-report and validated by the number of sexual chromosomes in whole genome sequencing data. Normal plasma cells were also retrieved from the femoral canal of individuals with isolated hip osteoarthritis who were otherwise healthy and signed informed consent. All samples were analyzed by whole genome sequencing (WGS) and single-nucleus Multiome, except MM-01-0221-t1 (bulk RNA sequencing only) and MM-01-0302-t1 (WGS only).

### **Myeloma and normal plasma cell purification**

Myeloma cells were purified from bone marrow or peripheral blood mononuclear cells using StraightFrom® Whole Blood and Bone Marrow CD138 MicroBeads (Miltenyi, ref.130-105-961) or FACS-sorted using a BD FACSAria III as CD38/CD319 positive and CD235a/CD3/CD33 negative (antibodies from Becton Dickinson, ref. 562444,564338,740785,555332 and 555450). Bone marrow mononuclear cells were purified from control bone marrow samples by Ficoll. Normal plasma cells were enriched by immunomagnetic sorting using anti-CD319 Antibody (Miltenyi, ref.130-099-575) and then FACS-sorted using the same procedure as myeloma cells.

### **Whole genome sequencing and analysis**

Genomic DNA was extracted from myeloma cells with NucleoSpin Tissue Kit (Macherey Nagel, 740952). Matched constitutional DNA was extracted from peripheral blood of the same patients with NucleoSpin Blood Kit (Macherey Nagel, 740951) or NucleoSpin Tissue Kit (Macherey Nagel, 740952). Tumor and constitutional DNA were sequenced at Integragen (Evry, France) on an Illumina NovaSeq 6000 as paired-end 150 bp reads, with an average depth of ~45-fold for tumors and ~30-fold for matched constitutional control samples, except for the two tumors of MM-01-0288 patient that were sequenced at 135X to identify minor subclones. We used Illumina DRAGEN software (v3.10.8) to align sequences on the hg38 version of the human genome and call somatic mutations. We then selected single nucleotide variants (SNVs) and indels with a DRAGEN flag equal to "PASS", or "weak\_evidence" with Tumor.SQ ≥ 10. To better assess the clonal evolution between t1 and t2 in MM-01-0288, we used bam-readcount (v1.0.0, <https://github.com/genome/bam-readcount>) to quantify the number of mutated reads in both samples for all mutations identified in either t1 or t2. This allowed to rescue variants identified in one sample and present in the other at low variant allele fraction

(VAF) hence not considered reliable by the variant caller. Only variants matching the following criteria were finally retained: sequencing depth  $\geq 8$  in the tumor and reference sample, VAF  $\geq 1\%$  in the tumor with  $\geq 3$  variant reads,  $\leq 1$  variant read in the control sample, and a VAF ratio  $> 5$  between the tumor and control samples. We used *Palimpsest*<sup>13</sup> to identify mutational signatures (from COSMIC database) operative in each sample. We used MANTA software<sup>14</sup> as implemented in DRAGEN to identify somatic structural variants (SVs). To keep only the most reliable events, we selected only SVs with the 'PASS' flag, supported by at least 10 reads in the tumor with a variant allele fraction  $\geq 10\%$ , and  $\leq 1$  variant read in the control sample. We used Facets R package (v0.6.2)<sup>15</sup> to reconstruct copy number profiles from WGS bam files of tumor and paired non-tumor liver samples. Single nucleotide polymorphisms (SNP) count matrices for tumor and non-tumor samples were obtained by processing the bam files with *snp-pileup*. We used *preProcSample* function to generate log-R-ratio (LRR) and B Allele Frequency (BAF) data from SNP matrices, *ProcSample* to estimate the wild-type 2-copy state and *emcncf* to estimate tumor ploidy, purity, allele specific copy-numbers and cellular fraction for each segmented chromosome segment. We used *Palimpsest* (v2.0.0)<sup>13</sup> to estimate the cancer cell fraction (CCF), i.e. the proportion of tumor cells carrying each mutation or SV, from its variant allele fraction, taking into account tumor purity and absolute copy number, as previously described<sup>16</sup>. We annotated alterations affecting multiple myeloma driver genes identified in previous studies<sup>17,18</sup>. We generated CIRCOS plots summarizing driver mutations, copy-number alterations and structural variants using a modified version of *RCircos* package (v1.2.2)<sup>19</sup>.

### Single-nucleus Multiome

Cryopreserved cells were thawed and nucleus permeabilization was performed following recommendations from 10X Genomics. Single-cell 3' gene expression and open chromatin libraries were simultaneously generated using Chromium Next GEM Single Cell Multiome ATAC + Gene Expression Kit (10X Genomics, ref.1000283) following the protocol provided by the manufacturer. A total of 12,000 nuclei were loaded per lane on the Chromium Single Cell Controller. Libraries were sequenced on a NovaSeq 6000 to a minimum depth of 250 million read pairs for Gene Expression library (Paired-end, 28bp Read 1, 90bp Read 2), and 163 million read pairs for ATAC library (Paired-end, 2\*50bp reads). We used *cellranger-arc* (v2.0)<sup>20,21</sup> to align snRNA-seq and snATAC-seq reads to the human genome (GrCh38/hg38) and generate the matrices of UMI counts per gene and ATAC-seq fragments. We modified the genes.gtf file used for snRNA-seq analysis by removing genes without HGNC ID that overlap HGNC genes. This prevents *cellranger-arc* from discarding reads overlapping well established protein-coding genes and non-coding RNAs (e.g. antisense), as *cellranger-arc* discards reads mapping to several genes in the gtf file. Our modified gtf included 35,010 genes (vs. 36,601 for the default gtf file).

### Single-nucleus RNA-seq analysis

We filtered the feature-barcode gene expression matrix to keep only high quality cells ( $>3000$  UMI counts,  $>1000$  genes detected and  $<15\%$  of mitochondrial reads) and expressed genes (detected in  $\geq 3$  cells). Detailed quality control metrics are provided in **Supplementary Table 7**. Secondary analyses were performed using *Seurat* package (v4.3.0)<sup>22</sup>. We used *SCTransform* with default parameters to normalize the filtered UMI count matrix. We generated UMAP (Uniform Manifold Approximation and Projection) visualizations of all cells from MM-01-0288 patient (t1 and t2,  $n=14,849$ ), and all cells from the 11 samples analyzed ( $n=65,700$ ). We first

used the 3,000 most variant genes to perform principal component analysis with *runPCA*, and ran Louvain graph-based clustering on the 50 first principal components before projecting the resulting data on a 2D UMAP with *runUMAP*. We used *FindNeighbors* and *FindClusters* with a resolution of 0.3 to identify transcriptomic clusters. We used *SingleR* (v1.8.1)<sup>23</sup> to annotate immune cell types, with the Single-Cell Tumor Immune Atlas reference available at <https://doi.org/10.5281/zenodo.4263972>. We removed cells with *SingleR* annotations other than "Plasma B cells", "Proliferative B cells" or "B cells", as well as cell clusters with low expression of plasma cell markers (*CD38*, *TNFRSF17*, *MZB1*, *PECAM1*, *SDC1*, *SSR4*, *TXNIP*, *XBP1*). These cells correspond to non-plasma cells that were not filtered out during sample preparation. We obtained on average 95.2% of plasma cells per sample. We used *InferCNV* package (version 1.9.1, <https://github.com/broadinstitute/infercnv>) with default parameters to reconstruct virtual copy-number profiles and identify tumor subclones with specific copy-number changes. Plasmocytes from normal bone marrow samples were used as reference cells, and genes with an average read count > 0.1 in reference cells were used for the analysis. We used the *Seurat FindMarkers* function (with Wilcoxon rank-sum test) for differential expression analyses. Genes with an adjusted p-value <0.05 and an absolute log fold-change >0.6 were considered significantly differentially expressed. We used *enrichR* R package (v.3.2) to identify pathways (from "KEGG\_2021", "Reactome\_2022", "WikiPathways\_2019" and "MSigDB\_hallmark\_2020" databases) significantly enriched (adjusted p-value <0.05) among differentially expressed genes.

### Single-nucleus ATAC-seq analysis

snATAC-seq data analysis was conducted with the *ArchR* package (v1.0.1)<sup>24</sup>. We first examined the distributions of the number of fragments per nucleus and transcription start site (TSS) enrichment in each sample, and we applied *ad hoc* filters (number of fragments > [10<sup>3.3</sup>-10<sup>3.7</sup>], TSS enrichment score > [12-14], adapted to each sample) to retain only the most reliable nuclei for further analysis. Detailed quality control metrics are provided in **Supplementary Table 7**. We used *ArchR addReproduciblePeakSet* function to identify chromatin accessibility peaks, with *MACS2*<sup>25</sup> method and grouping cells by sample. We used *ArchR getMarkerFeatures* function to identify peaks with differential accessibility (adjusted p-value <0.05 and |log<sub>2</sub>(fold-change)| > 1) between cells from the 2 GPRC5D-silenced relapses (MM-01-0221-t2 and MM-01-302-t2) vs. cells from other samples. We used *ArchR peak2genelinkage* function to identify peaks whose accessibility is correlated to the expression of GPRC5D among the 65,700 cells.

### Clonal evolution of MM-01-0288 myeloma

To reconstruct the clonal architecture of MM-01-0228, and its evolution between t1 and t2, we first compared the cancer cell fraction (CCF) of somatic mutations between the two time points (**Extended Data Fig. 6a**). K-means clustering revealed 3 subsets of mutations: trunk mutations (clonal in both t1 and t2), subclone A (dominant in t1 and minor in t2) and subclone B (minor in t1 but dominant in t2). Among driver alterations only the t(4;14) translocation and *ADCY2* mutation were trunk. *KRAS* G12R, *RB1* R787\* and *CDKN1B* N61I belonged to subclone A. *HUWE1* P3841L and *RB1* L572fs belonged to subclone B. Finally, *SF3B1* R1075K and the 7 alterations of *GPRC5D* were specific to t2 subclones, with CCF ranging from 6.2 to 31.6%. We used *SCReadCounts* (v1.3.1)<sup>26</sup> to detect somatic mutations in single-cell data, and we projected the number of mutated reads for each subset of mutations on the snRNA-seq UMAP (**Extended Data Fig. 6b,c**). As expected, trunk mutations were found in all cells. By contrast,

subclone A mutations were restricted to the major cell cluster in t1 and 2 minor cell clusters in t2. Subclone B mutations were restricted to the minor cell cluster in t1 and 3 cell clusters in t2. The proportion of cells harboring each mutation subset was consistent with the CCF estimated from WGS data. These data reveal which subclone in t1 gave rise to each subclone in t2, as represented by arrows in **Extended Data Fig. 6c**.

InferCNV's hierarchical clustering revealed 9 copy-number clusters (**Extended Data Fig. 8a**). Careful examination of WGS and InferCNV data revealed 6 reliable subclonal copy-number alterations (CNAs) in this patient: 4 identified by Facets in WGS data (-1p, -14q, -14qtel, +17q) and 2 (-10p, -21) detected in single-cell data only and clearly related to a specific subclone. We used InferCNV's ChromHMM tool to assign the status of each subclonal CNA in each cluster (**Extended Data Fig. 8b**). Of note, del14q (present in 77% of t2 cells according to Facets) was poorly detected by InferCNV. We thus used Numbat tool<sup>27</sup>, that takes into account SNP data in addition to expression ratios, to identify this alteration (**Extended Data Fig. 8c**). Finally, InferCNV clusters with identical copy-number profiles were merged to obtain the final classification in 5 copy-number subclones (**Fig. 1c** and **Extended Data Fig. 8d**). Copy-number subclones nicely matched transcriptomic clusters on the snRNA-seq UMAP and allowed us to refine the clonal architecture reconstructed from somatic mutations (**Fig. 2d**). Note that subclone cn5 appears as two transcriptomic clusters corresponding to cells in G1 versus cycling cells. Finally, we mapped *GPRC5D* alterations onto the snRNA-seq UMAP. Point mutations were identified with *scReadCounts* whereas reads harboring indels and supporting the deletion of exon 1 were manually identified in the bam files using the Integrative Genomics Viewer<sup>28</sup>. Each alteration was encountered in a single genetic subclone of the t2 sample: F158fs in cn4, S125fs in cn3 and all others in cn5 (**Fig. 2e**). Finally, we integrated mutations and copy-number alterations to reconstruct the relationships between genetic subclones, and the timing of acquisition of driver alterations. We used the *fishplot* package (v0.5.1)<sup>29</sup> to represent clonal evolution over time in patient MM-01-0288 (**Fig. 2f**).

### **Bulk RNA-seq**

We performed bulk RNA-seq for myeloma cells of MM-01-0221 (t1 and t2) and MM-01-0302 (t2). Total RNA was purified using direct-zol RNA MicroPrep kit (Ozyme, ZR2060) with on-column DNase treatment according to manufacturer's instructions. Libraries were generated from 200ng of total RNA using NEBNext Poly(A) mRNA Magnetic Isolation Module (New England Biolabs, E7490S) and NEBNext Ultra II Directional RNA Library Prep (New England Biolabs, E7765S). Libraries were sequenced on a NovaSeq 6000 as paired-end 100 bp reads. Full Fastq files were aligned to the reference human genome hg38 using *STAR* (V2.7.9a). We used *featureCount* to obtain the number of raw read counts associated to each gene in the ENSEMBL database (release-87 gtf file), and we calculated TPM scores (transcripts per millions of mapped reads) by normalizing the count matrix for the library size. We used COMMPASS RNA-seq data (<https://research.themmr.org>) to compare *GPRC5D* expression in MM-01-0221 and MM-01-0302 with a large series of multiple myelomas (bulk RNA-seq from 859 MM samples), as shown in **Fig. 2c**. We used two-sided Wilcoxon rank-sum tests to compare the expression of *GPRC5D* between molecular subgroups in the COMMPASS series.

### **Flow cytometry analysis of GPRC5D expression**

We detected the cell surface expression of GPRC5D in 2 cell lines (MM.1S cell line ATCC® CRL-2974 and NCI-H929 [H929] cell line ATCC® CRL-9068), 2 post-talquetamab relapses (MM-01-0288-t2 and MM-01-0221-t2, no cells left for MM-01-0302 after genomic analyses) and 4

other MM samples. Cryopreserved MM cell lines or myeloma cells were thawed and resuspended in staining mix with 5 mg/mL anti-GPRC5D antibody (571961 clone, R&D Systems) or corresponding isotype (IC0041P clone; R&D Systems). Samples were incubated for 60 minutes at room temperature. For multiple myeloma samples, cells were also stained with an antibody cocktail CD3/CD38/CD319/CD235a/DAPI (Becton Dickinson, ref. 560910,564499,56438 ; Biolegend, ref.306621). Cells were analyzed on a BD FACSAria III or Canto II cytometer using FlowJo software v10.9.0.

### **Statistics and reproducibility**

No statistical method was used to predetermine sample size. The sample size (3 patients) was chosen based on sample availability. These patients were not selected and correspond to the first 3 patients who relapsed after talquetamab at CHU Nantes with a bone marrow aspirate sufficiently rich in tumor cells to conduct whole genome and single-cell sequencing. No data were excluded from the analyses except poor quality cells (as explained in the 'Single-nucleus RNA-seq analysis' section). The experiments were not randomized. Data collection and analysis were not performed blind to the conditions of the experiments.

Further information on research design is available in the Nature Research Reporting Summary linked to this article.

### **Data availability**

Whole genome sequencing, bulk RNA-seq and single-cell Multiome data generated for this study have been deposited to the European Genome Archive (EGA accession number [EGAS00001007014](https://ega-archive.org/studies/EGAS00001007014)). These data contain identifiable genetic variants and are thus accessible under controlled access for patient privacy concerns, by contacting the data access committee. Source data for Fig. 1, 2 and Extended Data Fig. 1, 2, 3, 4, 5, 6, 7, 8, 9, 10 have been provided as Source Data files. All other data supporting the findings of this study are available from the corresponding author on reasonable request.

### **Code availability**

All bioinformatic tools used in this study are indicated in the relevant sections of the Material and Methods, with versions and modified parameters. Custom codes developed for this project have been deposited on Zenodo (DOI 10.5281/zenodo.8183942) and are available under open source Creative Commons Attribution 4.0 International license.

### **Acknowledgements**

This study was supported by the Région Pays de la Loire (Connect Talent program, RPH2114NNA), Nantes Métropole (RPH2114NNA), CHU Nantes, the I-SITE NexT (ANR-16-IDEX-0007), HéMA-NExT research cluster and the SIRIC ILIAD (INCa-DGOS-INSERM-ITMO Cancer\_18011). We thank the biological resource centre for biobanking (CHU Nantes, Hôtel Dieu, Tumorotheque, Nantes, F-44093, France). The authors acknowledge the Cytocell - Flow Cytometry and FACS core facility (SFR Bonamy, BioCore, Inserm UMS 016, CNRS UAR 3556, Nantes, France) for its technical expertise and help, member of the Scientific Interest Group (GIS) Biogenouest and the Labex IGO program supported by the French National Research Agency (n°ANR-11-LABX-0016-01). We warmly thank the patients who participated in this study.

## Author Contributions

E.L. conceived and directed the research. J.D., S.G., C.T. and E.L. designed the study and wrote the manuscript. E.D. and M.D. performed the experiments. J.D., S.G., F.M., S.M. and E.L. analyzed and interpreted the data. J.D., S.G., A.F., N.G., M.C., V.G., R.B. and E.L. performed bioinformatics and statistical analysis. P.M. and C.T. provided essential biological resources and collected clinical data. All authors approved the final manuscript and contributed to critical revisions to its intellectual context.

## Competing Interests

P.M. participates to the advisory boards and perceives honoraria from pharmaceutical companies producing multiple myeloma treatments: Janssen, celgene, abbvie, pfizer, amgen, sanofi, takeda. C.T. participates to the advisory boards and perceives honoraria from Janssen, the company that produces talquetamab. Other authors declare no competing interests.

## Figure Legends

**Figure 1. Polyclonal talquetamab resistance due to bi-allelic genetic inactivation of *GPRC5D*.** **a**, CIRCOS plots showing (from outer to inner layer) the driver mutations, copy-number changes and structural variants (abnormal junctions) identified by whole genome sequencing in the pre (left) and post-talquetamab (right) samples of patient MM-01-0288. **b**, *GPRC5D* mutations detected in the relapse are shown along *GPRC5D* protein sequence, with a color code indicating mutation consequence. The cancer cell fraction (proportion of tumor cells harboring the mutation) is indicated below each mutation. TSS: transcription start site. **c**, Virtual copy-number profiles reconstructed from single-nucleus RNA-seq data. Each row represents a cell, with regions of increased (resp. decreased) expression in red (resp. blue). The sample of origin of each cell is indicated on the left. Cells are grouped by their copy-number cluster (cn1 to cn5, right legend) identified by InferCNV tool. Subclonal copy-number changes are annotated and framed in the cn clusters in which they were detected. **d**, Projection of copy-number subclones onto the single-nucleus RNA-seq UMAP. Copy-number subclones nicely correlate with transcriptomic clusters. Note that subclone cn5 is split in two groups corresponding to cell cycle phases. **e**, Projection of *GPRC5D* alterations onto the single-nucleus RNA-seq UMAP. Each alteration is represented with a specific color code. As expected, *GPRC5D* alterations are encountered in t2 only. Each alteration is detected in a single copy-number cluster, indicating the subclone in which it appeared. **f**, Clonal evolution between pre-treatment sample (t1) and post-talquetamab relapse (t2). Driver mutations, t(4;14) translocation and copy-number changes are indicated. Copy-number subclones at t1 and t2 are colored as in panels c,d. *GPRC5D* mutations are colored as in panel e.

**Figure 2. Talquetamab resistance due to epigenetic inactivation of *GPRC5D* locus.** **a**, Clinical history of MM-01-0221 and MM-01-0302 patients. **b**, Gene expression (RNA-seq, top) and chromatin accessibility (ATAC-seq, bottom) at *GPRC5D* locus in normal bone marrow, MM-01-0221 and MM-01-0302-t2 tumor samples. MM-02-0221 and MM-02-0302 t1 samples could not be analyzed by ATAC-seq so another t(11;14) myeloma (MM-01-0286) is shown for comparison. Single-nucleus RNA-seq and ATAC-seq profiles of other normal bone marrow (BM) and MM samples are shown in **Extended Data Fig. 10c**, Bulk RNA-seq expression of *GPRC5D* in MM-01-0221 and MM-01-0302 samples as compared with the COMMPASS series (859 myelomas). While the expression in MM-01-0221 at t1 is close to the average in

COMMPASS, the expression in MM-01-0221 and MM-01-0302 t2 samples is extremely low. **d**, Large-scale epigenomic landscape around GPRC5D. Shown is a 500 kb region around *GPRC5D* with coordinated loss of many chromatin accessibility peaks (highlighted by red arrows). The upper panel shows the 3D interactions identified in B cells by promoter-capture Hi-C (Mifsud *et al.*). ATAC-seq data is shown for the 2 GPRC5D-silenced relapses (in red), 7 other MM samples (in blue) and 2 normal plasma cell samples (in green). MM ChIP-seq signals for H3K27Ac (enhancers), H3K36Me3 (transcribed genes) and H3K27Me3 (inactive chromatin) were obtained from BLUEPRINT database and are depicted below, together with the methylation level in normal bone marrow (BM). See also **Supplementary Table 5** for the complete definition and annotation of deregulated peaks.

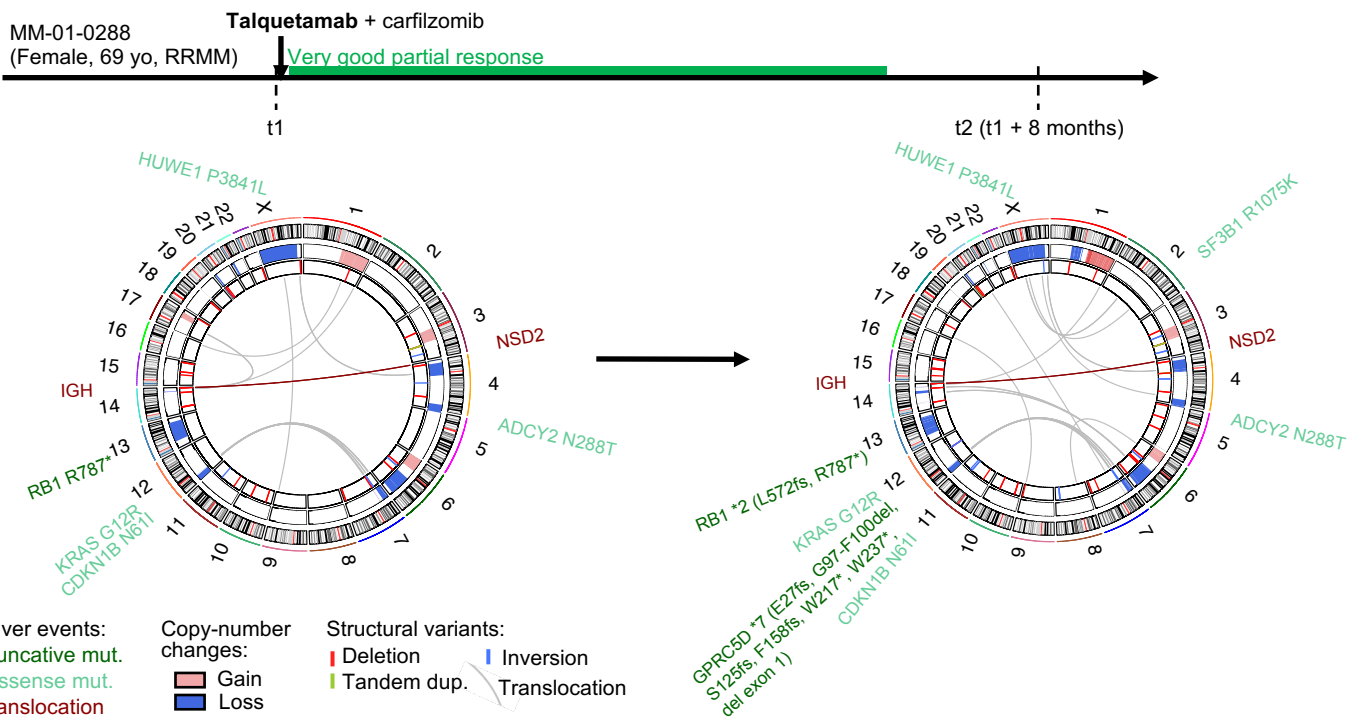
## References

1. Moreau, P. & Touzeau, C. T-cell-redirecting bispecific antibodies in multiple myeloma: a revolution? *Blood* **139**, 3681–3687 (2022).
2. Moreau, P. *et al.* Teclistamab in Relapsed or Refractory Multiple Myeloma. *New England Journal of Medicine* **387**, 495–505 (2022).
3. Chari, A. *et al.* Talquetamab, a T-Cell–Redirecting GPRC5D Bispecific Antibody for Multiple Myeloma. *New England Journal of Medicine* **387**, 2232–2244 (2022).
4. Benaniba, L. *et al.* The MYRACLE protocol study: a multicentric observational prospective cohort study of patients with multiple myeloma. *BMC Cancer* **19**, 855 (2019).
5. Moore, J. E. *et al.* Expanded encyclopaedias of DNA elements in the human and mouse genomes. *Nature* **583**, 699–710 (2020).
6. Mifsud, B. *et al.* Mapping long-range promoter contacts in human cells with high-resolution capture Hi-C. *Nat Genet* **47**, 598–606 (2015).
7. Fishilevich, S. *et al.* GeneHancer: genome-wide integration of enhancers and target genes in GeneCards. *Database (Oxford)* **2017**, bax028 (2017).
8. Da Vià, M. C. *et al.* Homozygous BCMA gene deletion in response to anti-BCMA CAR T cells in a patient with multiple myeloma. *Nat Med* **27**, 616–619 (2021).
9. Samur, M. K. *et al.* Biallelic loss of BCMA as a resistance mechanism to CAR T cell therapy in a patient with multiple myeloma. *Nat Commun* **12**, 868 (2021).
10. Maclachlan, K. H. *et al.* Copy number signatures predict chromothripsis and clinical outcomes in newly diagnosed multiple myeloma. *Nat Commun* **12**, 5172 (2021).
11. Hon, G. C. *et al.* Global DNA hypomethylation coupled to repressive chromatin domain formation and gene silencing in breast cancer. *Genome Res.* **22**, 246–258 (2012).

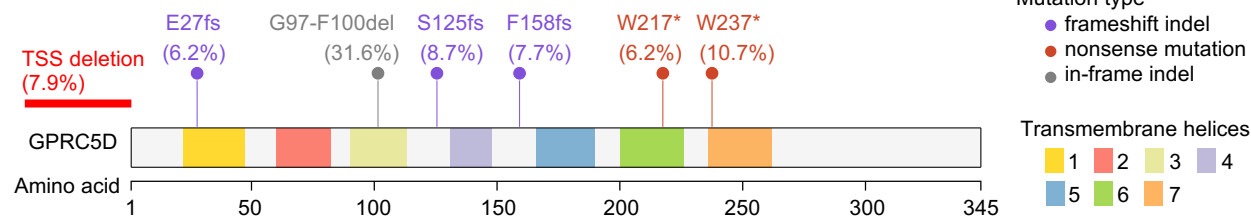
## Online Methods references

12. Kumar, S. *et al.* International Myeloma Working Group consensus criteria for response and minimal residual disease assessment in multiple myeloma. *Lancet Oncol* **17**, e328–e346 (2016).
13. Shinde, J. *et al.* Palimpsest: an R package for studying mutational and structural variant signatures along clonal evolution in cancer. *Bioinformatics* **34**, 3380–3381 (2018).
14. Chen, X. *et al.* Manta: rapid detection of structural variants and indels for germline and cancer sequencing applications. *Bioinformatics* **32**, 1220–1222 (2016).
15. Shen, R. & Seshan, V. E. FACETS: allele-specific copy number and clonal heterogeneity analysis tool for high-throughput DNA sequencing. *Nucleic Acids Res* **44**, e131 (2016).

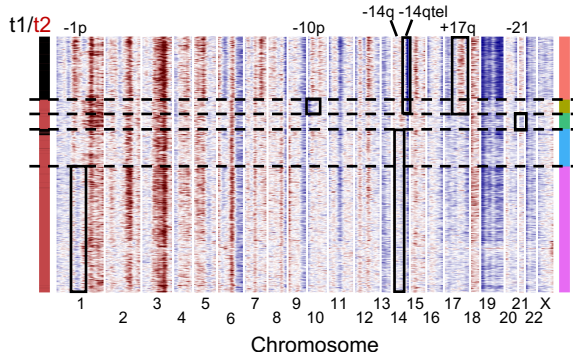
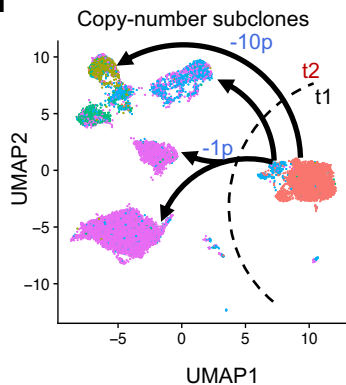
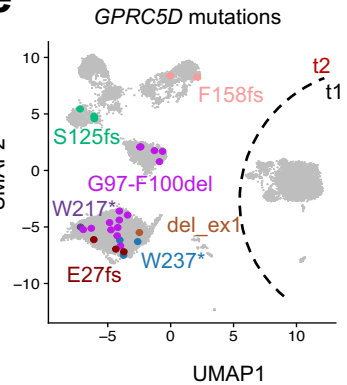
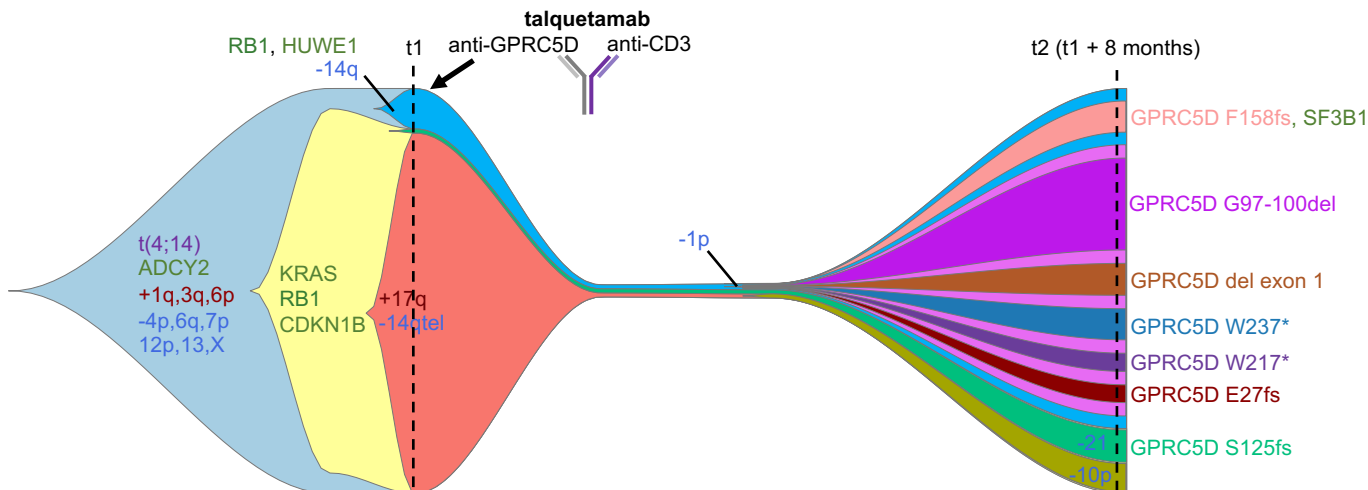
16. Letouzé, E. *et al.* Mutational signatures reveal the dynamic interplay of risk factors and cellular processes during liver tumorigenesis. *Nat Commun* **8**, 1315 (2017).
17. Walker, B. A. *et al.* Identification of novel mutational drivers reveals oncogene dependencies in multiple myeloma. *Blood* **132**, 587–597 (2018).
18. Barwick, B. G. *et al.* Multiple myeloma immunoglobulin lambda translocations portend poor prognosis. *Nat Commun* **10**, 1911 (2019).
19. Zhang, H., Meltzer, P. & Davis, S. RCircos: an R package for Circos 2D track plots. *BMC Bioinformatics* **14**, 244 (2013).
20. Zheng, G. X. Y. *et al.* Massively parallel digital transcriptional profiling of single cells. *Nature Communications* **8**, 14049 (2017).
21. Satpathy, A. T. *et al.* Massively parallel single-cell chromatin landscapes of human immune cell development and intratumoral T cell exhaustion. *Nat Biotechnol* **37**, 925–936 (2019).
22. Stuart, T. *et al.* Comprehensive Integration of Single-Cell Data. *Cell* **177**, 1888–1902.e21 (2019).
23. Aran, D. *et al.* Reference-based analysis of lung single-cell sequencing reveals a transitional profibrotic macrophage. *Nat Immunol* **20**, 163–172 (2019).
24. Granja, J. M. *et al.* ArchR is a scalable software package for integrative single-cell chromatin accessibility analysis. *Nat Genet* **53**, 403–411 (2021).
25. Zhang, Y. *et al.* Model-based Analysis of CHIP-Seq (MACS). *Genome Biology* **9**, R137 (2008).
26. Prashant, N. M. *et al.* SCReadCounts: estimation of cell-level SNVs expression from scRNA-seq data. *BMC Genomics* **22**, 689 (2021).
27. Gao, T. *et al.* Haplotype-aware analysis of somatic copy number variations from single-cell transcriptomes. *Nat Biotechnol* **41**, 417–426 (2023).
28. Robinson, J. T. *et al.* Integrative genomics viewer. *Nat Biotechnol* **29**, 24–26 (2011).
29. Miller, C. A. *et al.* Visualizing tumor evolution with the fishplot package for R. *BMC Genomics* **17**, 880 (2016).

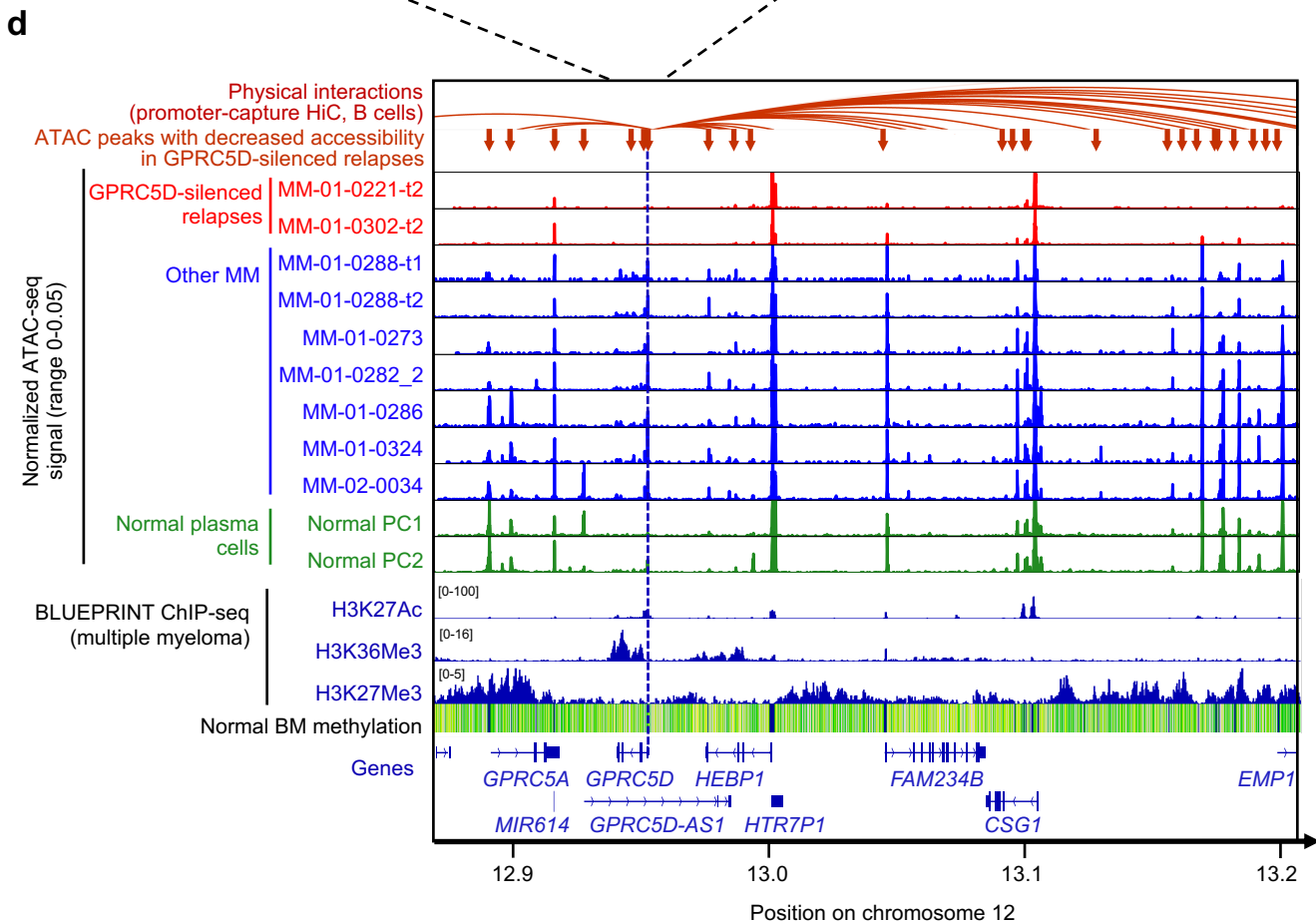
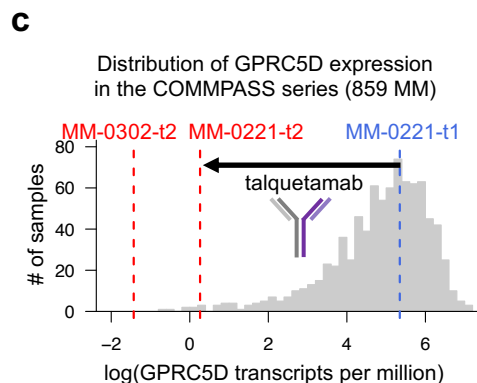
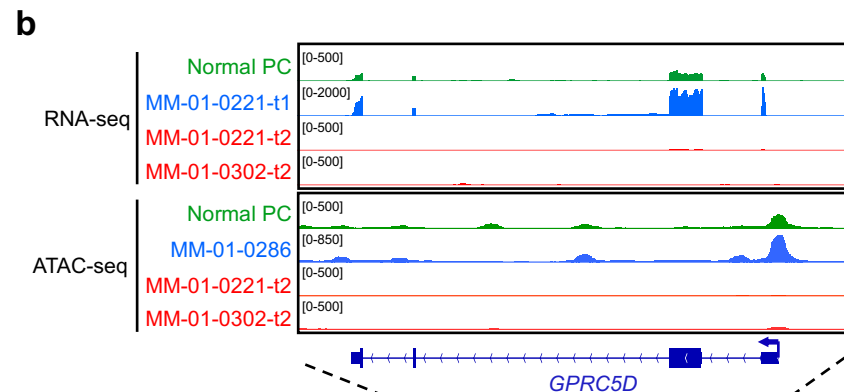
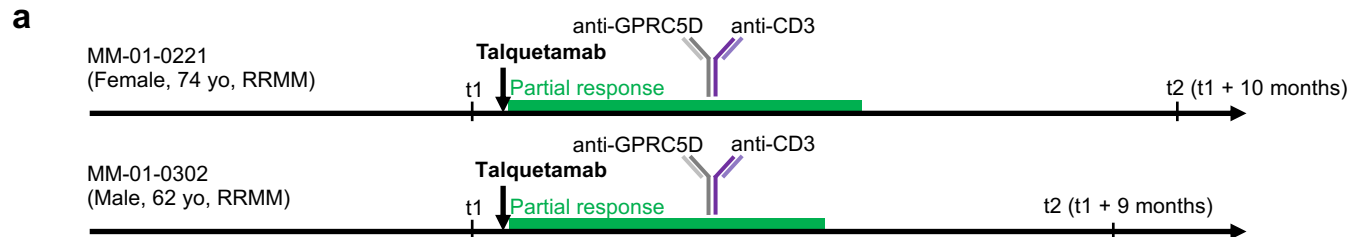
**a****b**

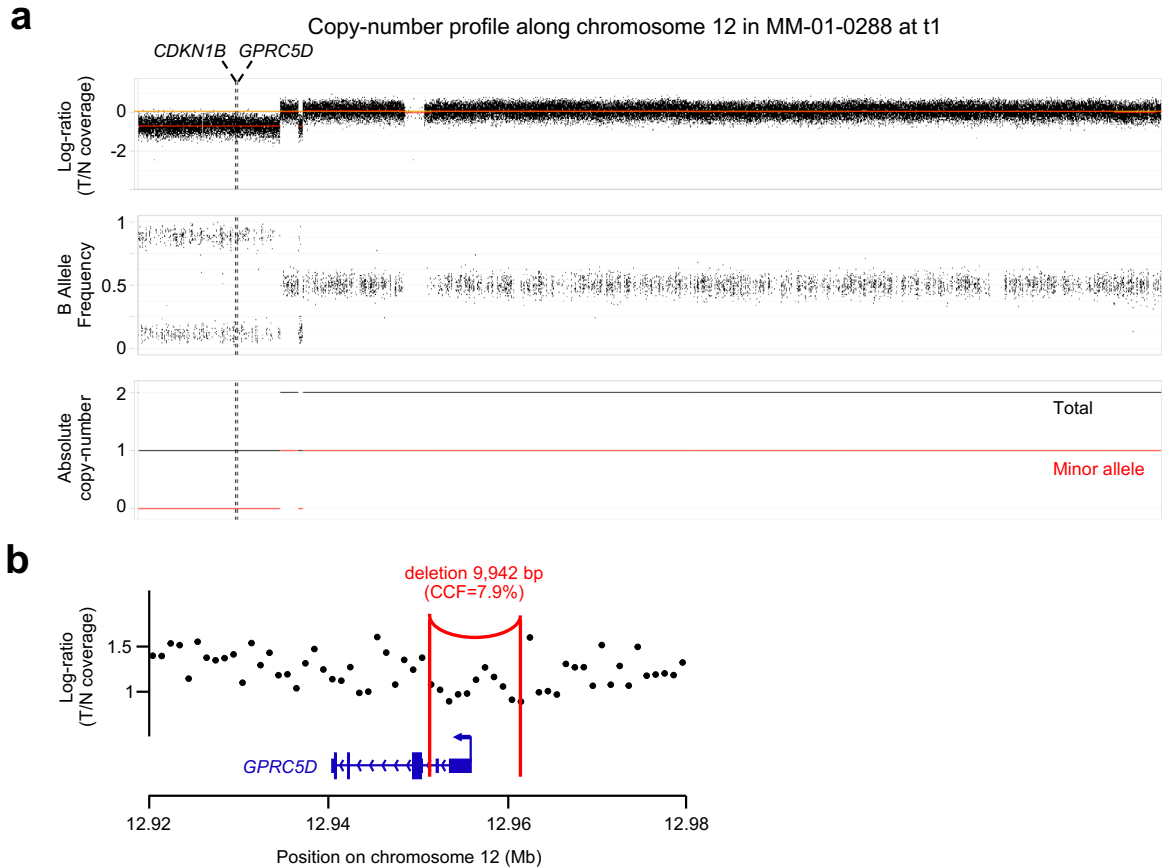
Subclonal GPRC5D mutations identified in MM-01-0288-t2 (Cancer Cell Fraction)

**c**

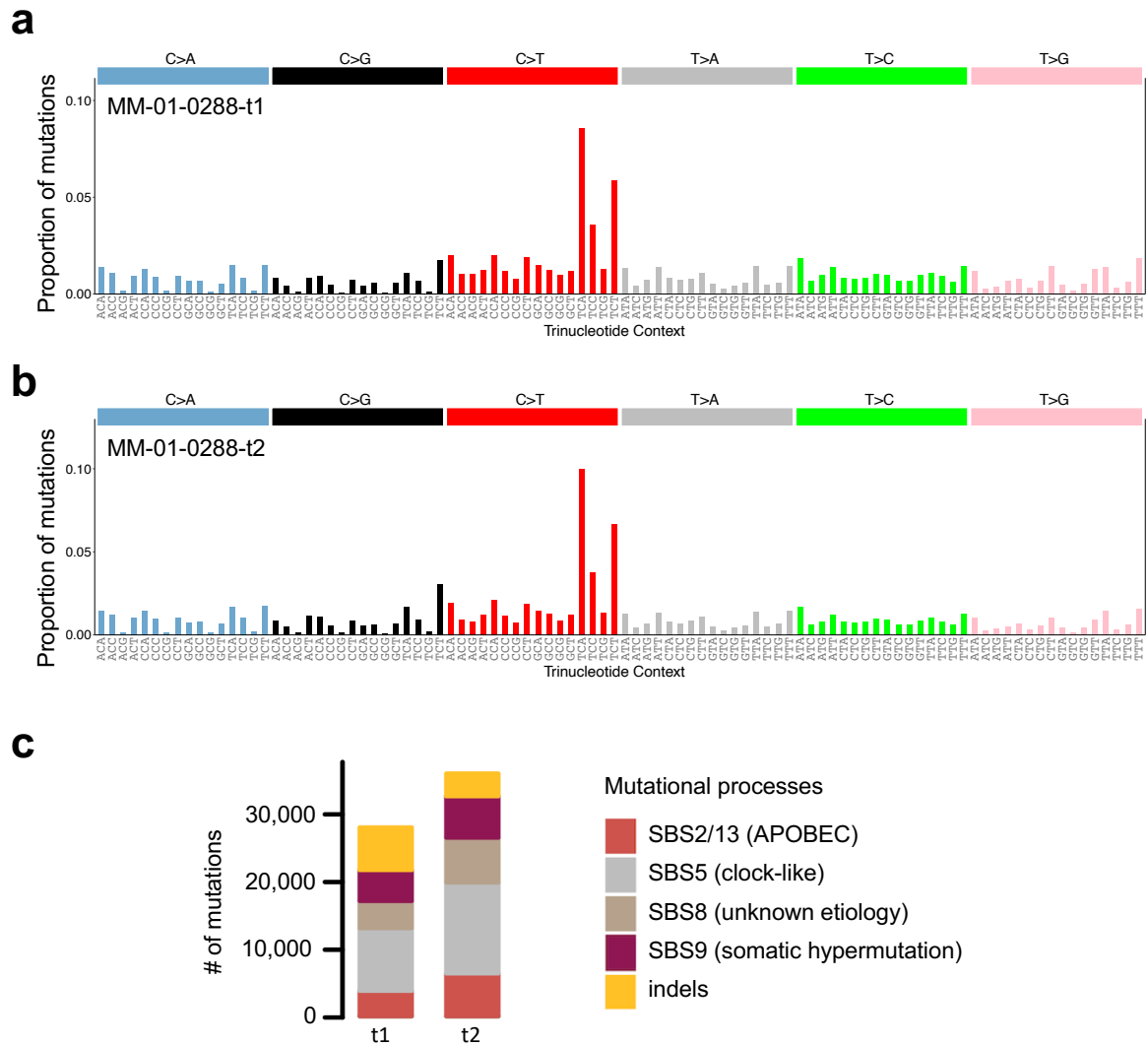
Single-cell copy-number profiles (t1 & t2, 14,849 cells)

**d****e****f**

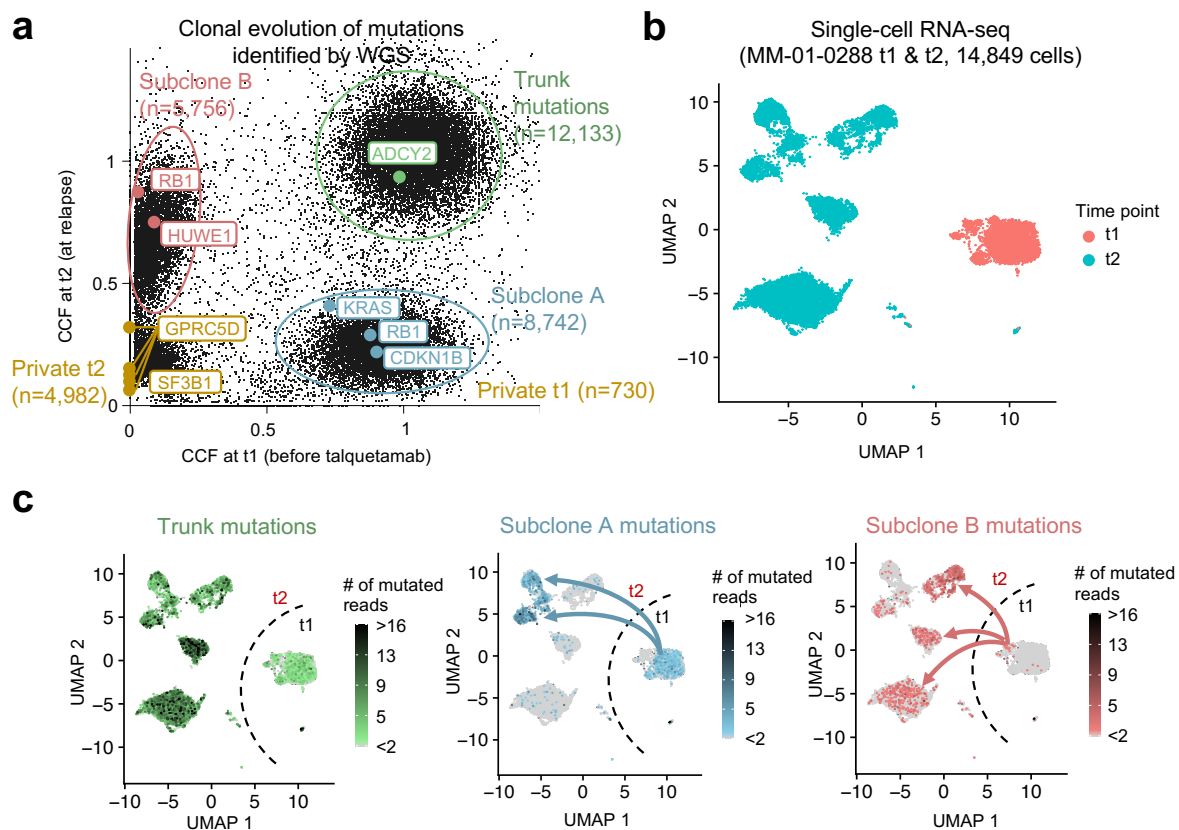




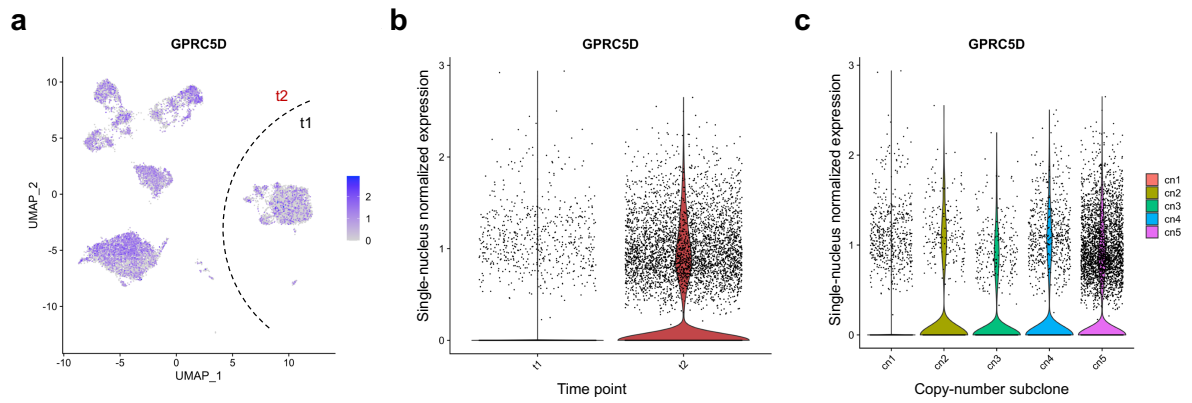
**Extended Data Fig. 1 - Chromosome 12p deletion and structural variant affecting GPRC5D in MM-01-0288.** **a**, Copy-number profile along chromosome 12 in MM-01-0288-t1 sample, showing a deletion on the 12p arm encompassing *CDKN1B* and *GPRC5D*. Upper panel: coverage log-ratio between the tumor and normal samples. Middle: B Allele Frequency of common polymorphisms. Bottom: Absolute copy-number estimated by FACETs algorithm. The location of *CDKN1B* and *GPRC5D* genes is shown with dashed lines. **b**, Focal deletion encompassing the transcription start site of *GPRC5D*, identified in 7.9% of cells of MM-01-0288-t2.



**Extended Data Fig. 2 - Mutational signature analysis of tumors MM-0288-t1 and t2.** Proportion of the 96 mutation categories in MM-01-0288-t1 (a) and t2 (b). We can distinguish a high prevalence of C>T mutations in TCA and TCT contexts, characteristic of APOBEC mutagenesis. c, Deconvolution of COSMIC mutational signatures in MM-01-0288 t1 and t2 samples.

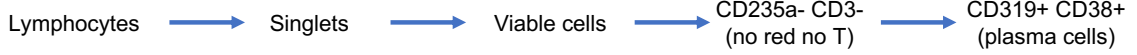


**Extended Data Fig. 3 - Integration of WGS and single-cell data reveals the clonal evolution of MM-01-0288.** **a**, Clonality of somatic mutations identified by whole genome sequencing in MM-01-0288. Each point represents a mutation, with its cancer cell fraction (CCF) in t1 on the x-axis, and in t2 on the y-axis. Trunk mutations (CCF  $\sim 1$  in both t1 and t2) are highlighted, together with two subclones: subclone A (dominant in t1 and minor in t2) and subclone B (minor in t1 and dominant in t2). Private mutations encountered in only one sample are located on the axes. In addition to these, 4,049 mutations were identified with low CCF in both samples. **b**, Uniform Manifold Approximation and Projection (UMAP) of the 14,849 cells analyzed from MM-01-0288 t1 and t2 samples. Each point represents a cell. They are grouped according to the similarity of their transcriptomic profiles, and colored by sample of origin. **c**, Projection of somatic mutations identified by WGS onto single-cell RNA-seq UMAs. For each set of mutations, the total number of mutated reads per cell is represented with a color code. Trunk mutations are detected in all cells. Subclone A mutations are detected in the major subclone of t1 and 2 minor subclones of t2. Subclone B mutations are detected in the minor subclone of t1 and 3 subclones of t2. The proportion of cells harboring each set of mutations is consistent with their CCF estimated from WGS data in each tumor.

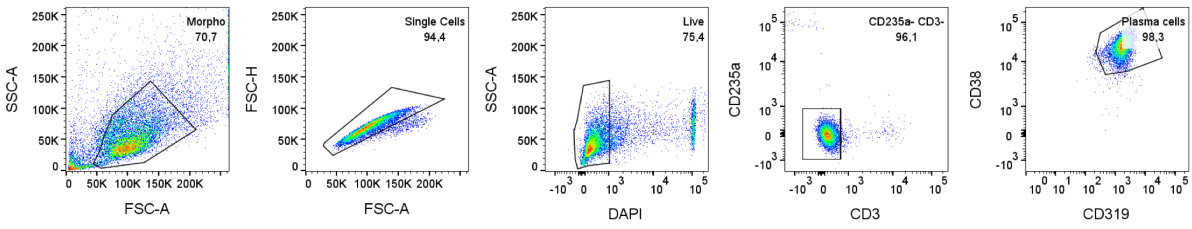


**Extended Data Fig. 4 - Single-cell GPRC5D mRNA expression in MM-01-0288.** **a**, Projection of GPRC5D mRNA expression onto the single-nucleus RNA-seq UMAP of patient MM-01-0288. **b**, Violin plot showing the distribution of single-nucleus GPRC5D expression in cells from t1 and t2 time points. **c**, Violin plot showing the distribution of single-nucleus GPRC5D expression in the 5 copy-number subclones.

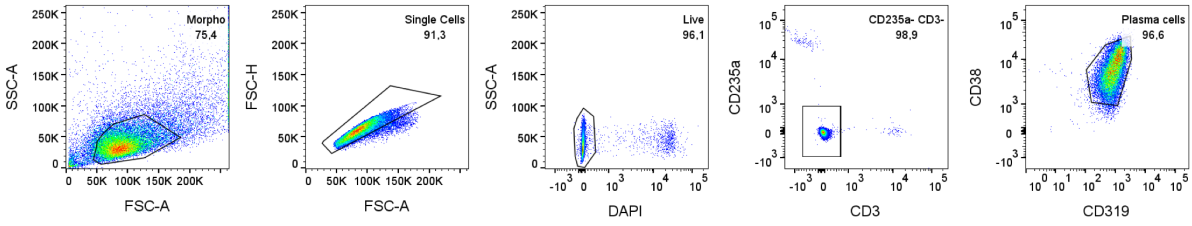
**Gating strategy**



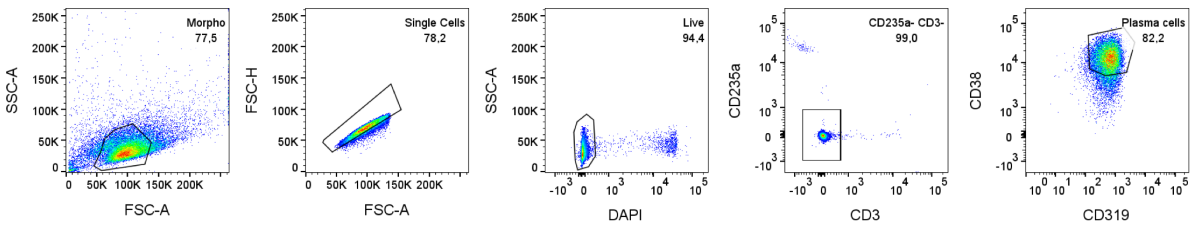
**MM-01-0264**



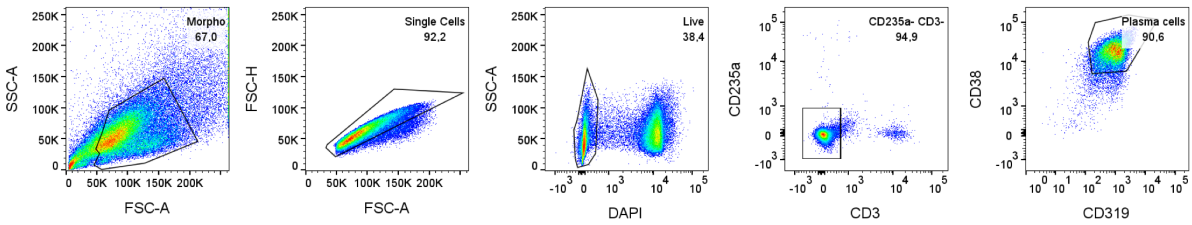
**MM-02-0034**



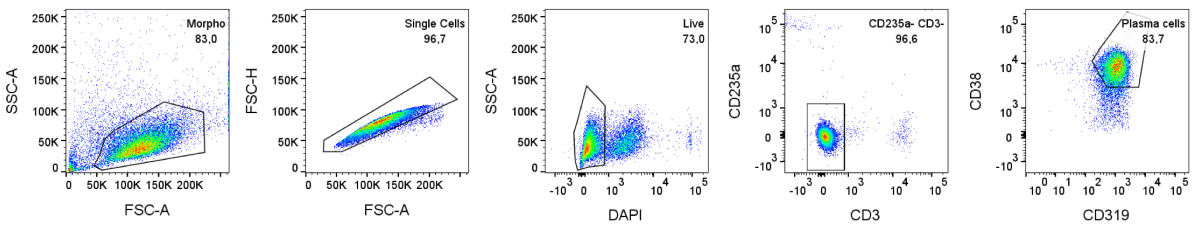
**MM-01-0282**



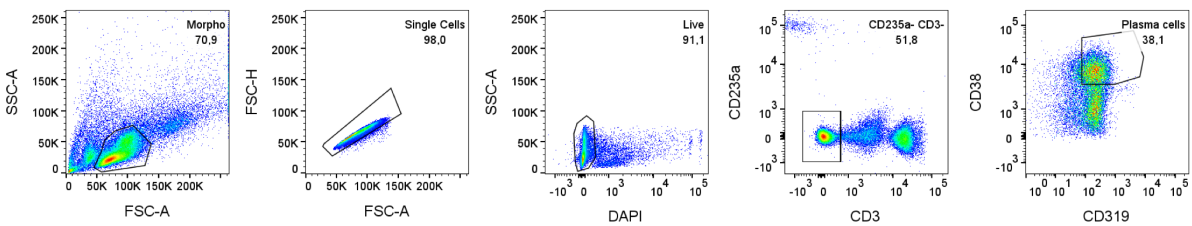
**MM-Epi-112**



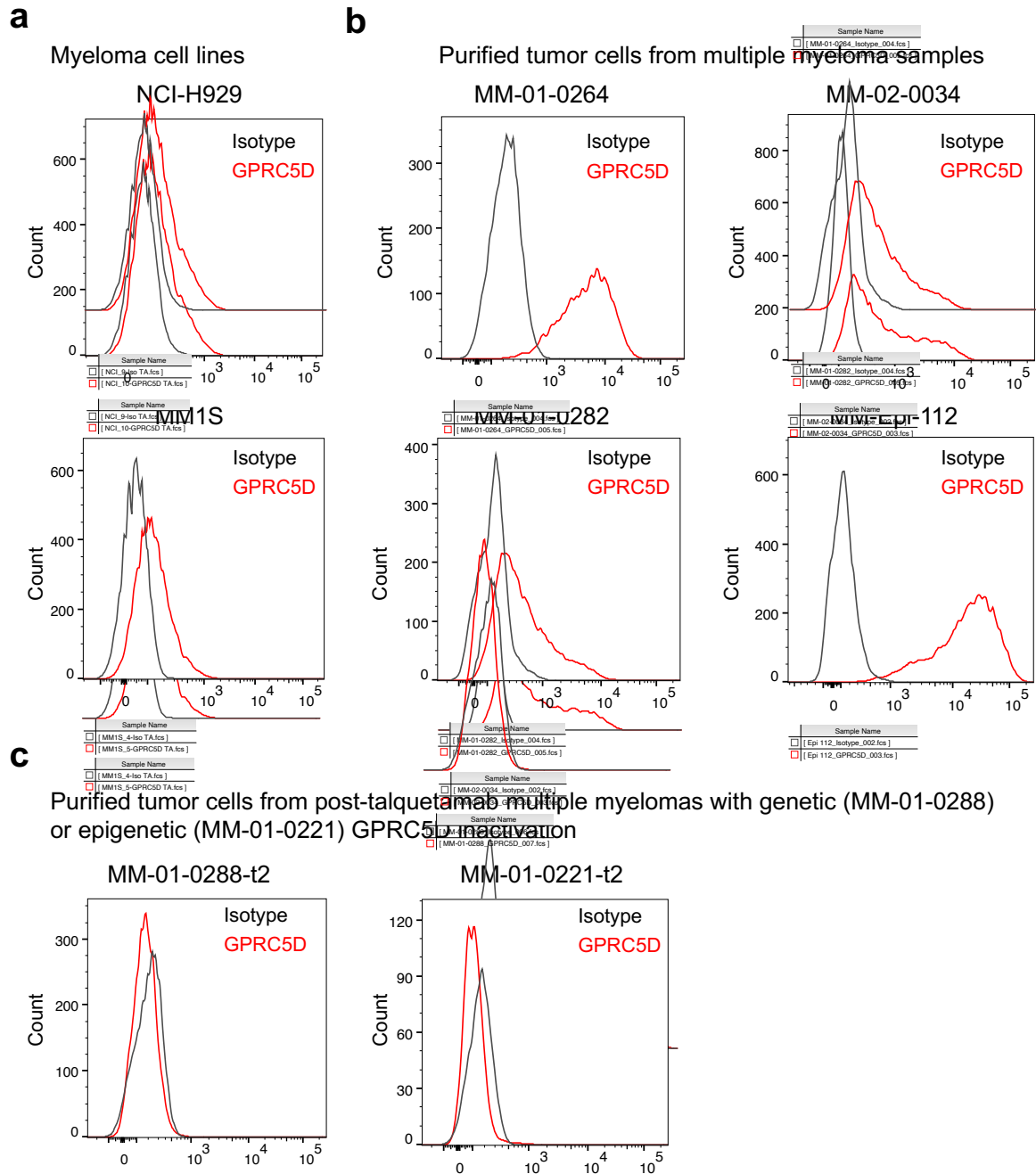
**MM-01-0288-t2**



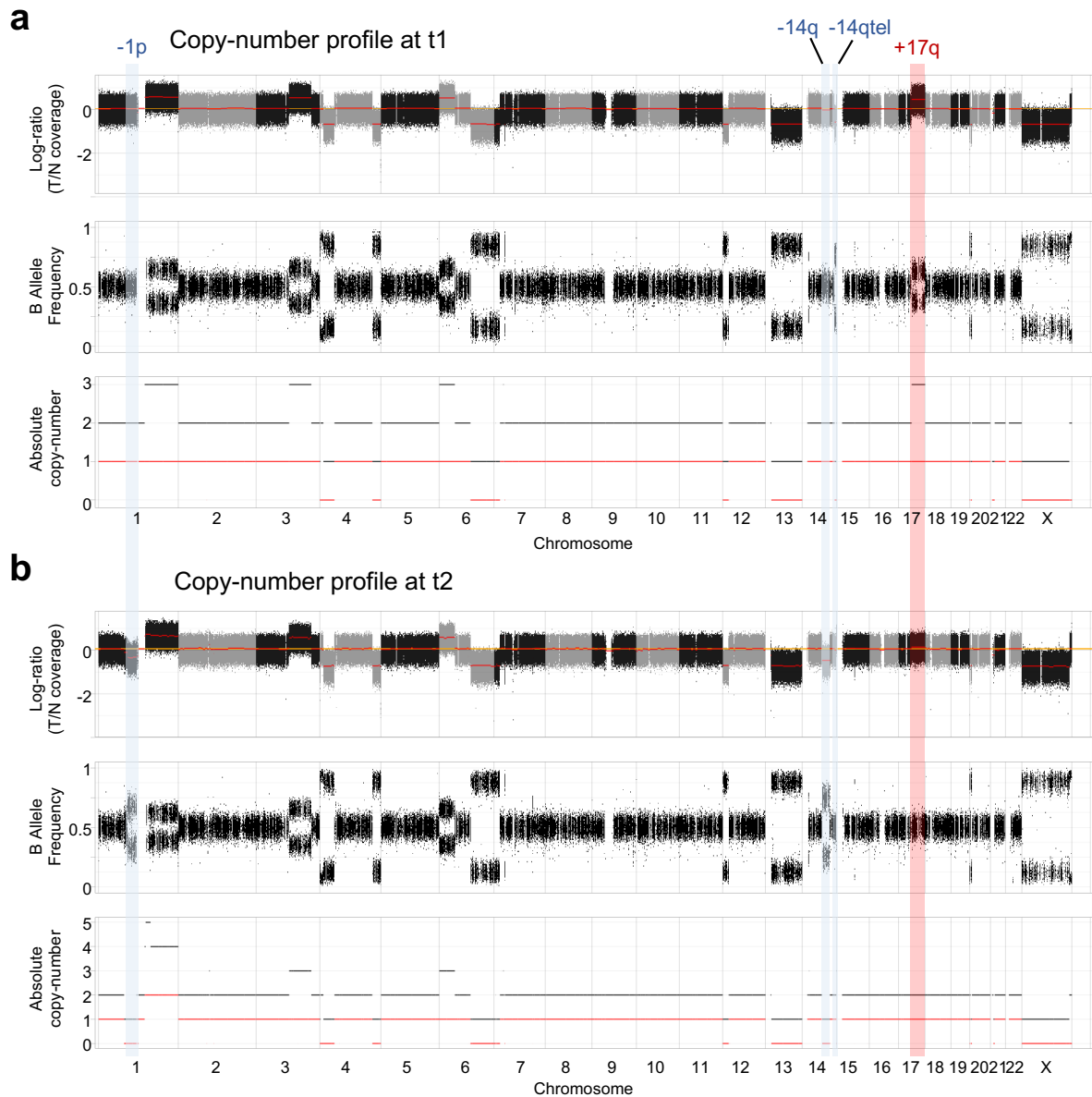
**MM-01-0221-t2**



**Extended Data Fig. 5 - Flow cytometry gating.** The gating strategy is shown on top and the results for each sample below.



**Extended Data Fig. 6 - Cell surface protein expression of GPRC5D analyzed by flow cytometry.** GPRC5D cell-surface protein expression was analyzed in 2 MM cell lines (**a**), sorted tumor cells from 4 multiple myelomas (**b**) and sorted tumor cells from multiple myelomas with genetic (MM-01-0288) or epigenetic (MM-01-0221) inactivation of GPRC5D (**c**). Cells were labeled using an anti-GPRC5D antibody (red line; 571961 clone; R&D Systems) or an isotype control antibody (gray line; IC0041P clone; R&D Systems) for 60 minutes at 4°C and analyzed by flow cytometry.

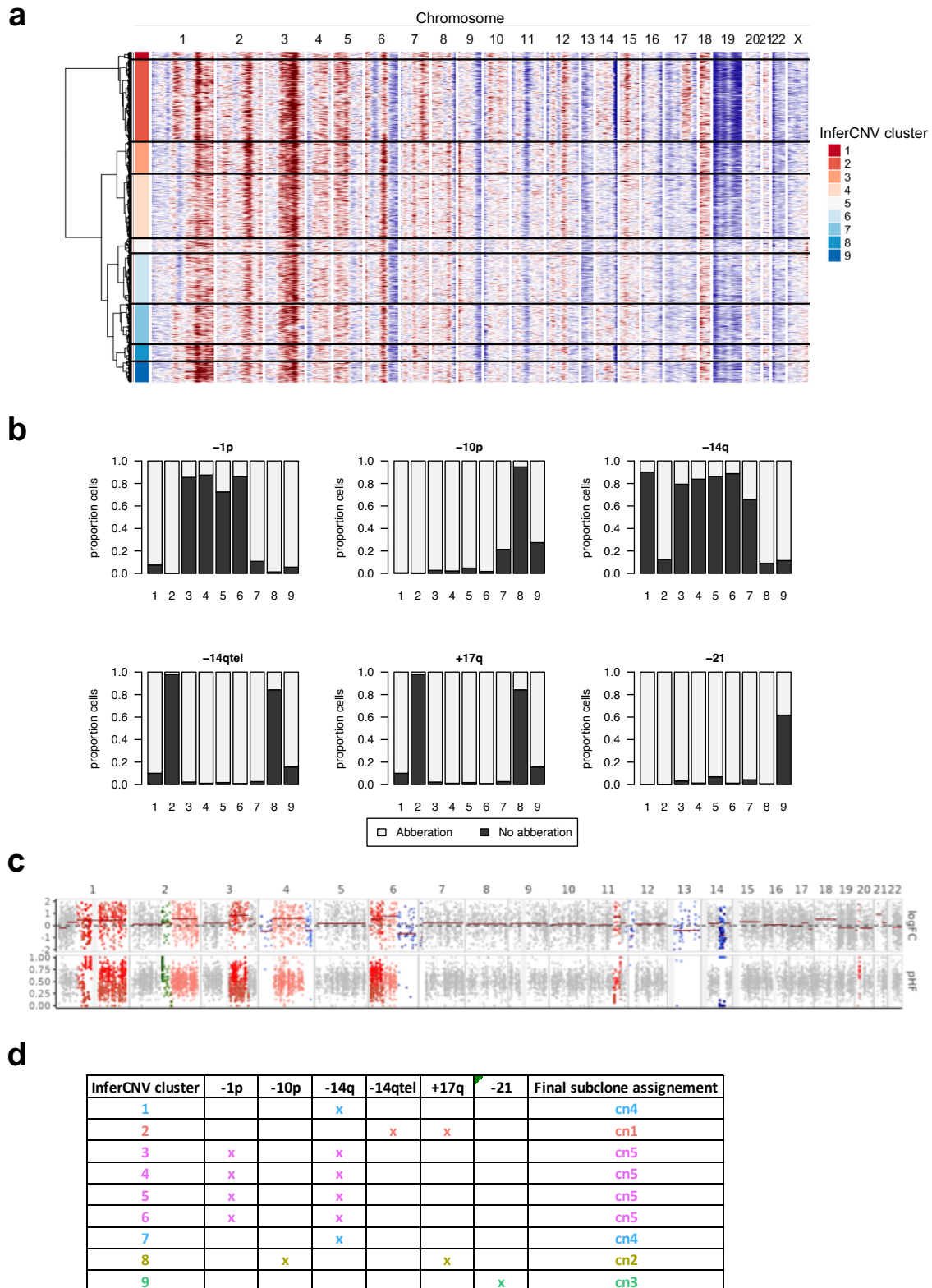


**c** Subclonal copy-number alterations identified by WGS

Name	start position	end position	start cytoband	end cytoband	CCF at t1	CCF at t2
-1p	91154593	118662000	1p22.2	1p12	0%	62%
-14q	62077000	86049057	14q23.2	14q31.3	<20%	77%
-14qtel	100911369	105744692	14q32.31	14q32.33	91%	<20%
+17q	41325100	83237000	17q21.2	17qtel	81%	<20%

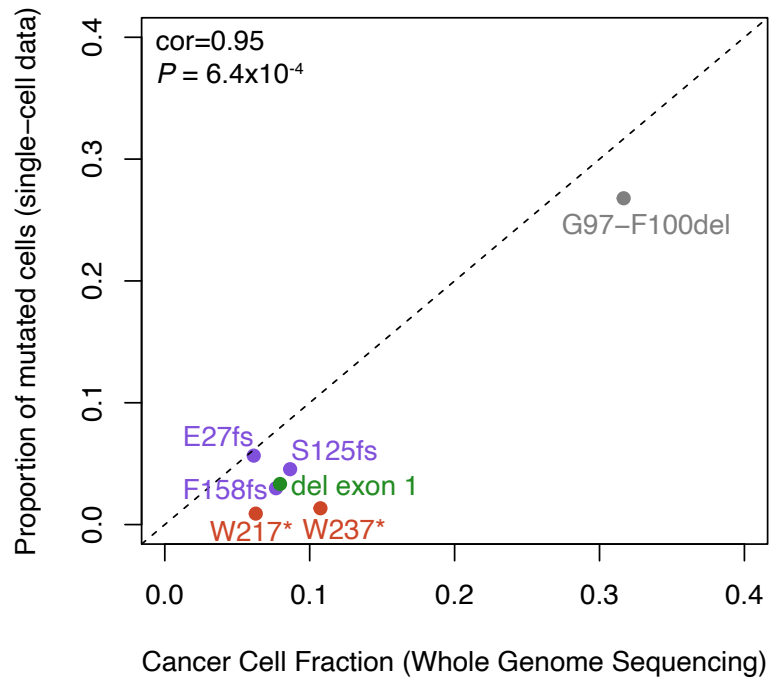
**Extended Data Fig. 7 - Clonal and subclonal copy-number changes identified by whole genome sequencing in MM-01-0288.** Pangenomic copy-number profiles of MM-01-0288 before (a) and after (b) talquetamab treatment. The two samples display 10 common clonal copy-number changes : +1q, +3q, -4p, -4q, +6p, -6q, -7p, -12p, -20p and -X.. One aberration (-1p) is absent in t1 and subclonal in t2, and 3 aberrations (-14q, -14qtel and +17q) are subclonal with different cancer cell fractions (CCF) in each sample. Subclonal copy-number number losses and gains are highlighted in blue and red, respectively. For each sample, the upper panel shows the coverage log-ratio between the tumor and normal samples, the middle panel shows the B Allele Frequency of common polymorphisms, and the bottom panel shows the absolute copy-number estimated by FACETS algorithm. c, Detailed characterization of subclonal copy-

number changes, including the detailed coordinates and the cancer cell fraction (CCF, e.g. proportion of tumor cells harboring the alteration) at t1 and t2. We indicated a CCF "<20%" for alterations visible on the profile but below FACETs detection threshold.

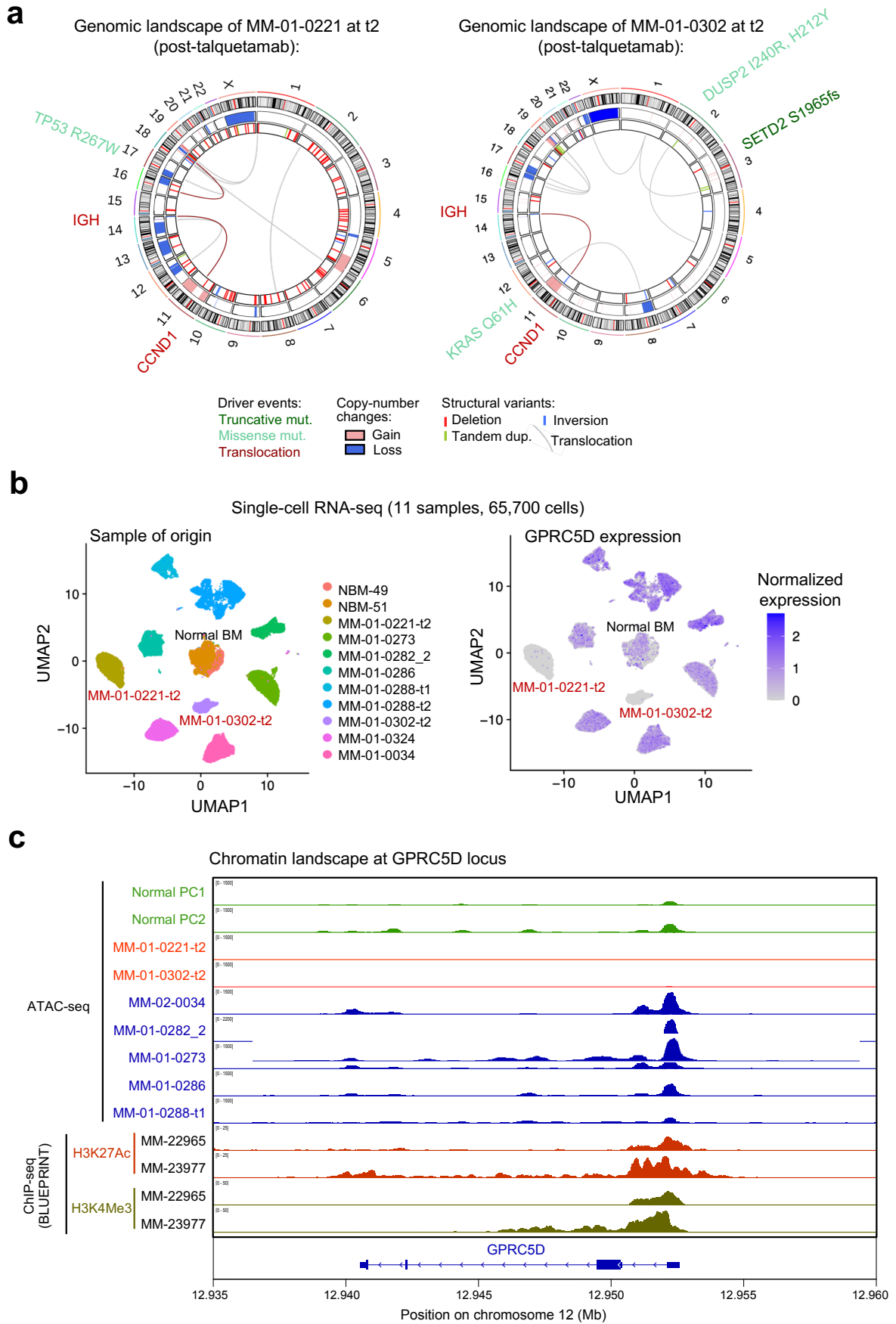


**Extended Data Fig. 8 - Identification of 5 copy-number subclones in MM-01-0288.** **a**, Unsupervised classification by hierarchical clustering as implemented in InferCNV (Ward.D method) reveals 9 clusters. **b**, Proportion of cells within each cluster carrying each of the 6 reliable subclonal CNAs identified in the patient. We used InferCNV HMM predictions to determine the presence of aberrations in each cell, except for the -14q deletion that was identified using Numbat tool. **c**, Numbat identifies in single-cell data a subclone carrying the

same 14q deletion identified by FACETs in WGS data. The upper track shows the log(fold-change) of expression in cells of the subclone vs. reference cells, and the bottom track shows the allele frequencies of polymorphisms. **d**, Assignment of final copy-number subclones. InferCNV clusters with identical copy-number profiles were merged: InferCNV 1 and 7 into cn4, InferCNV 3-6 into cn5.



**Extended Data Fig. 9 - Proportion of cells carrying each GPRC5D alteration identified by WGS and single-cell sequencing data.** The type of alteration is highlighted by a color code. The p-value and correlation score were obtained using Pearson's correlation test.



**Extended Data Fig. 10 - Genomic landscape and regulation of GPRC5D in the two post-talquetamab relapses with epigenetic silencing. a, CIRCOS plot showing (from outer to inner**

layer) the driver mutations, copy-number changes and structural variants identified by whole genome sequencing in the post-talquetamab sample of patient MM-01-0221. **b**, UMAPs showing the classification of 65,700 cells from 11 samples (2 normal bone marrow samples and 9 multiple myelomas) based on their snRNA-seq profiles. Cells are colored according to their sample of origin (left) or their level of *GPRC5D* expression (right). **c**, Chromatin landscape at *GPRC5D* locus. ATAC-seq signals are showing two normal bone marrow samples (in green), the 2 *GPRC5D*-silenced post-talquetamab relapses MM-01-0221-t2 and MM-01-0302-t2 (in red) and 5 other MM samples (in blue), together with H3K27Ac (enhancer mark) and H3K4Me3 (promoter mark) ChIP-seq signals in 2 MM samples from BLUEPRINT project. All samples display a major peak of accessibility at *GPRC5D* promoter, and up to 5 minor peaks in the gene body. All loci are closed in MM-01-0221-t2 and MM-01-0302-t2, as demonstrated by the lack of ATAC-seq reads. The ATAC-seq peak overlapping *GPRC5D* promoter has both H3K27Ac and H3K4Me3 marks in BLUEPRINT samples, consistent with an active promoter role. Other ATAC-seq peaks match H3K27Ac peaks, indicating their putative enhancer role.